An Ultrasound Image Despeckling Approach Based on Principle Component Analysis

Jawad F. Al-Asad   *jalasad@pmu.edu.sa*
Department of Electrical Engineering
Prince Mohammad Bin Fahd University
Al Khobar, P.O. Box 1664, 31952, Saudi Arabia

Ali M. Reza   *reza@uwm.edu*
Department of Electrical Engineering and Computer Science
University of Wisconsin-Milwaukee
Milwaukee, United States of America

Udomchai Techavipoo   *udomchai@gmail.com*
National Electronics and Computer Technology Center
Pathumthani, Thailand

Abstract

An approach based on principle component analysis (PCA) to filter out multiplicative noise from ultrasound images is presented in this paper. An image with speckle noise is segmented into small dyadic lengths, depending on the original size of the image, and the global covariance matrix is found. A projection matrix is then formed by selecting the maximum eigenvectors of the global covariance matrix. This projection matrix is used to filter speckle noise by projecting each segment into the signal subspace. The approach is based on the assumption that the signal and noise are independent and that the signal subspace is spanned by a subset of few principal eigenvectors. When applied on simulated and real ultrasound images, the proposed approach has outperformed some popular nonlinear denoising techniques such as 2D wavelets, 2D total variation filtering, and 2D anisotropic diffusion filtering in terms of edge preservation and maximum cleaning of speckle noise. It has also showed lower sensitivity to outliers resulting from the log transformation of the multiplicative noise.

Keywords: Covariance Matrix, Denoising, Despeckling, Principle Component Analysis, Ultrasound Imaging.

1. INTRODUCTION

Ultrasound medical imaging is considered to be cost efficient and practically harmless to the human body. However, the quality of medical ultrasound images is degraded by the presence of speckle noise. Images acquired by pulse-echo ultrasound systems demonstrate the interaction between the incident pressure field and the spatial inhomogeneities of the medium [1]. The majority of such spatial inhomogeneities in soft tissue is highly concentrated with the dimensions much smaller than the wavelength of the incident pressure waves and can be modeled as diffuse scatterers, which radiate the incident acoustic energy in all directions. The large concentration of small scattering targets with sub-wavelength dimensions gives rise to a characteristic pseudo-random granular texture in the envelope-detected image known as speckle. Unlike other kinds of noise, speckle noise is not strictly random but is rather an intrinsic feature of soft tissue. Multiple scans of the same region that are taken in the same position with the same probe and under the same conditions will, in the absence of electrical noise, yield exactly the same speckle pattern each time [1].

Despite the negative effect on the quality of ultrasound images, speckle also carries clinically

important textural information that can be useful for tissue identification [2]. Therefore, methods for image restoration aimed at improving the diagnostic utility of ultrasound images need to enhance image resolution and improve image clarity while preserving the textural information present in the speckle.

In literature, various speckle noise reduction methods have been proposed [3]–[12]. Averaging filters and adaptive weighted median filters [5] are simple and effective noise reduction methods. By introducing weight coefficients to the well known median filter and adjusting the smoothing characteristics of the filter, it is possible to effectively suppress noise. However, such schemes seem to remove fine details being actually filters with a low-pass characteristic [6].

Wavelet denoising is applied for despeckling in medical ultrasound imaging [2], [4], [7], [11], [12]. It is based on multiscale decompositions. It consists of three main steps. First, the noisy signals are analyzed using a wavelet transform. Then the empirical wavelet coefficients are shrunk. Finally, denoised signals are synthesized from these shrunk coefficients through the inverse wavelet transform. These methods are generally referred to as wavelet shrinkage techniques [1]. It is found to be the best approach among many denoising methods in synthetic aperture radar (SAR) images [3]. In [4], logarithmic transformation is used to convert the multiplicative noise to an additive noise prior to wavelet denoising. These are referred to as the homomorphic wavelet despeckling (HWDS) methods [4]. In [11], a non-Gausian statistical model with an adaptive smoothing parameter is used in the wavelet transformed domain. It was shown that the HWDS does not improve the signal-to-noise ratio (SNR) [8] because the wavelet transformed speckle coefficients are larger than the threshold value, thus not suitable for removing the speckle noise in ultrasound images. Moreover, the log transformed multiplicative noise is spiky in nature, following Fisher-Tippett distribution [6]. HWDS tends to preserve such spikes unless it is properly treated. Two preprocessing stages have been proposed to solve this problem [6]. The first stage is to decorrelate the speckle noise samples. This stage requires point spread function estimation from the ultrasound envelope image. The second stage applies the median filter to normalize the distribution of the log transformed spiky noise. These stages improve the noise distribution to be more Gaussian that is suitable for most wavelet denoising schemes. In [7], adaptive decorrelation is used for further image enhancement.

Total variation filtering (TVF) [10] and anisotropic diffusion filtering (ADF) [9] are also used for despeckling. Similar results can be obtained via replacing the wavelet denoising step proposed in [6] by TVF and ADF. TVF is useful for recovering constant signals and it is considered to be among the most successful methods for image restoration and edge enhancement. It is mainly because of its capability of filtering out the noise without blurring the most universal and crucial features of image edges. Adversely, ADF takes advantage of the locality and anisotropy diffusion. It is capable of smoothing images with a decreased blur of the boundaries between their homogenous regions. ADF was shown to perform well for images corrupted by additive noise. However, in cases where images contain speckle noise, ADF enhances that noise instead of eliminating it [13].

Principle component analysis (PCA) is applied to reduce speckle noise in SAR images [14], [15] PCA is a result from linear algebra [16]. It arises from the eigen decomposition of the covariance matrix of the signals. It is used for dimensionality reduction and compression of multidimensional data. Unlike many despeckling techniques that trade spatial information for noise reduction, using PCA reduces speckle noise with minimal loss of spatial resolution. The first few principal components hold significant spatial information, while higher order components are dominated by speckle [14].

In this paper, a PCA-based approach for despeckling medical ultrasound images is explored and analyzed in detail. The approach is first introduced in [17]. PCA is applied through overlapped

segments of the ultrasound images. After log transformation, a global covariance matrix is formed by averaging the corresponding covariance matrices of the segments. A projection matrix is then calculated by selecting few principal eigenvectors of the global covariance matrix. This projection matrix is used to filter the speckle noise from the ultrasound images. The PCA-based approach is applied to simulated and real ultrasound images and the despeckling results are compared to those from HWDS, TVF, and ADF approaches in terms of the resolution, edges, and the signal to speckle noise ratio.

2. ULTRASOUND SIGNAL MODEL

A generalized model of a speckle noisy image is given by [18]

$$g(n,m) = f(n,m)u(n,m) + \xi(n,m) \qquad (1)$$

where g, f, u, and ξ stand for the observed envelope image, original image, and multiplicative and additive components of the speckle noise, respectively. The n and m respectively denote the axial and lateral indices of the image samples, or alternatively, the angular and radial indices for the sector images. This model has been successfully used both in ultrasound and SAR imaging. When applied to ultrasound images, this model can be simplified by disregarding the additive noise term. This leads to the following model:

$$g(n,m) \approx f(n,m)u(n,m) \qquad (2)$$

Consequently, adopting (2) as the basic model, it is assumed that the image g(n, m) is observed before the system processing is applied [6].

2.1 Proposed Algorithm

In the implementation of the proposed PCA-based approach to despeckle ultrasound envelope images, subtracting the mean before despeckling and adding it afterward is avoided. Through experimentations, it shows that subtracting the mean can be more beneficial for additive noise rather than a log transformed multiplicative noise. The non-linear logarithmic transformation for conversion of the multiplicative noise into additive noise is done globally at the beginning rather than for each segment (block). This method is found to have a positive impact on the quality of the denoised images compared to the method of transforming segments individually.

The following algorithm summarizes the steps implementing the concept of PCA-based approach in despeckling ultrasound envelope images. Assuming that the size of the ultrasound envelope images is $n \times m$, where n and m are the numbers of pixels in the axial and lateral directions, respectively.

Step 1: Apply logarithmic transformation to the given image.

Step 2: Segment the image into overlapping segments s_i, each of $q \times p$ size, where i is the index of the segment; and q and p are the numbers of pixels in the axial and lateral directions, respectively. The segmentation can be done laterally or axially across the 2D image. Segment s_{i+1} is shifted by one pixel from segment s_i.

Step 3: Reshape s_i into a column vector v_i of $q.p \times 1$ size and find a covariance matrix c_i of the vector v_i, such that $c_i = v_i \times v_i^T$, where T denotes transposition.

Step 4: Sum all c_i and average them by the number of segments of the image to get the overall covariance matrix (R) for the whole image. This method of averaging all covariance matrices of the segments serves to represent various speckle developments within the image, thus yielding a better estimation of the global (overall) covariance matrix.

Step 5: Calculate the eignevalues and eigenvectors of R. Select $k < q.p$ eigenvectors that correspond to the set of largest eigenvalues. The remaining $q.p - k$ eigenvectors are simply rejected or ignored. The largest eigenvalues and the corresponding eigenvectors contribute to the true signal in the presence of noise.

Step 6: Form a feature matrix F by sorting the k selected eigenvectors according to their corresponding eigenvalues in the descending order. The size of the feature matrix F is now $q.p \times k$. This sorting procedure enables the use of the eigenvectors that correspond to the true signal.

Step 7: Calculate the transformation or the global projection matrix $P = F \times F^T$.

Step 8: Calculate a denoised vector d_i by projecting v_i onto the projection matrix P, i.e., $d_i = P \times v_i$.

Step 9: Reshape the denoised vector d_i back to a segment of the size of $q \times p$.

Step10: Reconstruct the envelope image by averaging all the overlapping denoised segments according to their original locations and the number of pixels superimposed on each coordinate, and take the exponential.

2.2 Image Quality Measures

To assess the denoising capabilities, we apply five image quality measures: α, β, SNR, S-SNR, and PSNR. These measures are defined as follows. Let I_{org} be the noise free original image and I_{est} be the estimated image or the image after denoising. First, the measure α is the ratio of the number of pixels of the estimated image's autocorrelation function ($R_{Iest\ Iest}(\tau_n, \tau_m)$, where τ_n and τ_m are the lags in n and m indices, respectively) that exceeds 75% of its maximum value to the total number of pixels. This α is mostly used to evaluate the resolution in ultrasound imaging [6]. Lower α usually implies better image resolution. Second, the measure β is used to assess the ability of the despeckling methods to preserve sharp details of the images. It is given by [19] as

$$\beta = E\left\{ \frac{\left\langle \Delta I_{org}, \Delta I_{est} \right\rangle}{\left\| \Delta I_{org} \right\|_F \left\| \Delta I_{est} \right\|_F} \right\} \tag{3}$$

where Δ is the Laplacians operator; $\langle \cdot, \cdot \rangle$ denotes the standard inner product; E{ . } is the expectation; and || . ||F is the Frobenius matrix norm, i.e., $\left\| I(n,m) \right\|_F = \sqrt{\sum_n \sum_m \left| a_{nm} \right|^2}$. The β closer to 1 indicates the better despeckling ability in preserving image edges. Third, the SNR is the conventional signal to noise ratio which is defined as $E\left\{ \left\| I_{org} \right\|_F / \left\| I_{org} - I_{est} \right\|_F \right\}$. Fourth, the S-SNR is the speckle signal to noise ratio. It is defined as the mean to the standard deviation of the estimated image I_{est}. S-SNR is an indicator of the degree of contamination of the image by the speckle noise. Finally, the PSNR is the peak signal to noise ratio. It is the most commonly used measure of quality in image denoising. The PSNR is given by

$$PSNR = E\left\{ \max \left| I_{org} \right|^2 / \left\| I_{org} - I_{est} \right\|_F \right\} \tag{4}$$

For simulations, the β, SNR, S-SNR, and PSNR are used. Due to the absence of the original image in case of real ultrasound data, only α and S-SNR can be applied. The SNR, S-SNR, and PSNR can be reported in dB unit by taking $10 \log_{10}(.)$ of their values.

3. RESULTS, CRITICAL DISCUSSION AND COMPARATIVE EVALUATION

3.1 Simulated Phantom Image

The Field II Program [20], [21] is used to simulate ultrasound envelope images in this paper. Although the Field II program does not account for nonlinear propagation of the ultrasound wave with higher harmonics, which in return improve the quality of the image, the simulated image from the program is used to compare the despeckling approaches. To test denoising efficiency, sharp edges and curves are included within the simulated image as shown in Fig. 1. The image also includes low, medium, and high scattering areas, as represented by dark, white, and background areas, respectively. We simulate 128 radiofrequency (RF) echo signals using 5625 scatterers per cm^2 with a lateral resolution of 0.156 mm. This number of scatterers is chosen in accordance with the simulations made in [20], [22]. The envelopes of the RF echo signals are obtained by taking the absolute value of the Hilbert transformation of the RF echo signals [23]. All of the envelopes are rearranged side-by-side to form a 2D envelope image. The envelope image is decimated in the axial direction from 1024 to 256 to yield a 256×128 image, as shown in Fig. 1-a. The corresponding speckle noisy version, shown in Fig. 1-b, is created by corrupting the undecimated envelope image by noise according to equation 2.
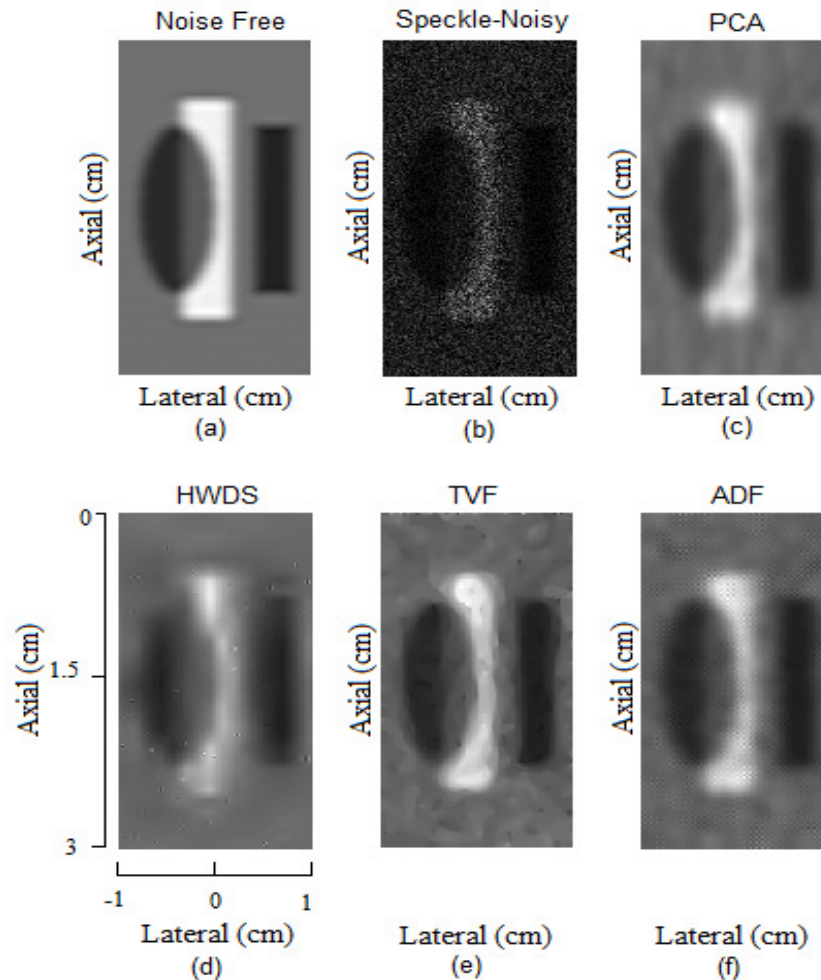

FIGURE 1: Simulated phantom images: a noise-free envelope image (a), a speckle noisy image (b), and the images after despeckling using PCA (c), HWDS (d), TVF (e), and ADF (f) methods. Note that the horizontal and vertical axes represent the axial and lateral axes, respectively (the images are transposed).

The PCA-based approach is compared to three nonlinear despeckling schemes, HWDS, TVF, and ADF. For HWDS, the WaveLab® package (Department of Statistics, Stanford University) is

used. HWDS is applied with four-level wavelet decomposition and Daubechies with four vanishing moments. Since the objective in this paper is not to compare various thresholding schemes, the original approach in [24] is used. The noise variance is estimated by assuming that most empirical wavelet coefficients at the finest level of decomposition are induced by the noise. TVF is also used to include the best empirically adjusted parameters for yielding the best visual results and for avoiding image blurring. The regularization parameter (λ) controls how much smoothing is performed, large noise levels call for large λ. TVF uses 100 iterations and $\lambda = 400$. ADF uses 35 iterations and a conduction coefficient of 25. Speed of diffusion controlled by λ is set to the maximum ($\lambda = 0.25$). The option of favoring wide regions over smaller ones is chosen for the ADF. The proposed PCA-based approach is used with a segment size of 16×8 and one eigenvector or written in short as (16/8-1). The images after being despeckled using PCA, HWDS, TVF, and ADF methods are shown in Fig. 1-c to Fig. 1-f, respectively. According to the plots in Fig. 1, the edge preservation and maximum cleaning of the speckle noise can be seen through the proposed approach as compared to the other denoising schemes.

The plots in Fig. 2 compare the performance measures averaged over 100 independent trials. As can be seen, the proposed PCA-based approach provides higher β, SNR, and PSNR than the other methods. However, the S-SNR from the proposed approach comes in the second place after that from the HWDS.
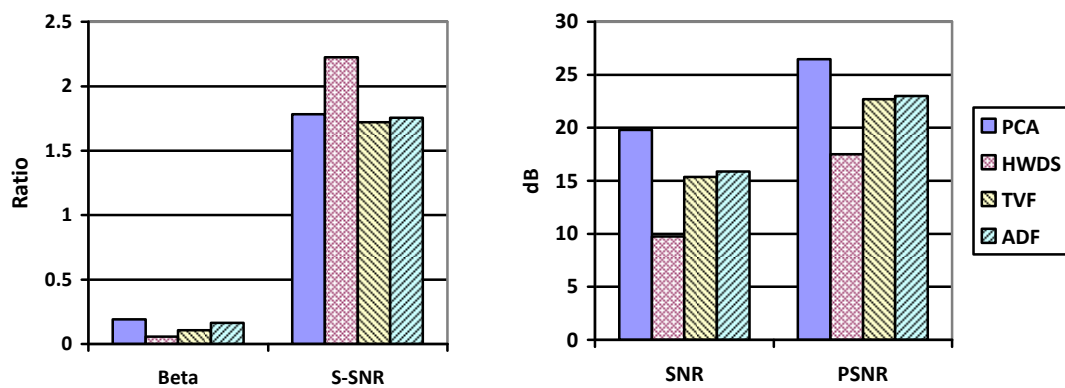

FIGURE 2: Performance comparison of denoising schemes when applied to the simulated phantom image. Vertical axis represents the magnitude in dB for SNR and PSNR while the magnitude is of no unit for Beta and S-SNR.

The comparisons of the axial and lateral profiles are shown in Fig. 3 and Fig. 4, respectively. These profiles are taken from the centers of the images in Fig. 1. The profiles plotted in Fig. 3 and Fig. 4 are from the original (a) and noisy (b) images, and the images after despeckled using the PCA (c), HWDS (d), TVF (e), and ADF (f) methods. The profile from the original image in (a) is also plotted as dotted lines on the same axes of the profiles from the despeckled images in (c) to (f). It is clear from these figures that our PCA-based approach has provided the closest profiles to the original ones. In agreement with the results provided in (Yu and Acton 2002), Fig. 3-f and Fig.4-f also show that the ADF method is less efficient in removing the speckle noise. Notice a remaining spike in the profile around the 70th pixel in Fig. 3-d, a drop-off in the profile around the 120th pixel in Fig. 3-e, and noisy profiles in Fig. 3-f and Fig. 4-f, compared to a smooth profile that follows the original profile closely in Fig. 3-c and Fig. 4-c. From these figures, it implies that the PCA-based approach is insensitive to spikes. The insensitivity of the PCA-based approach to the log transformed spiky noise is also observed by comparing Fig. 1-c with Fig. 1-d.

To further investigate the number of principle components used in our PCA-based approach, the parameters (16/8-1) are changed to (16/8-2), (16/8-3), and (16/8-4). Fig. 5 displays the results. It

shows that the higher the number of eigenvectors, the more the speckle noise becoming dominant.
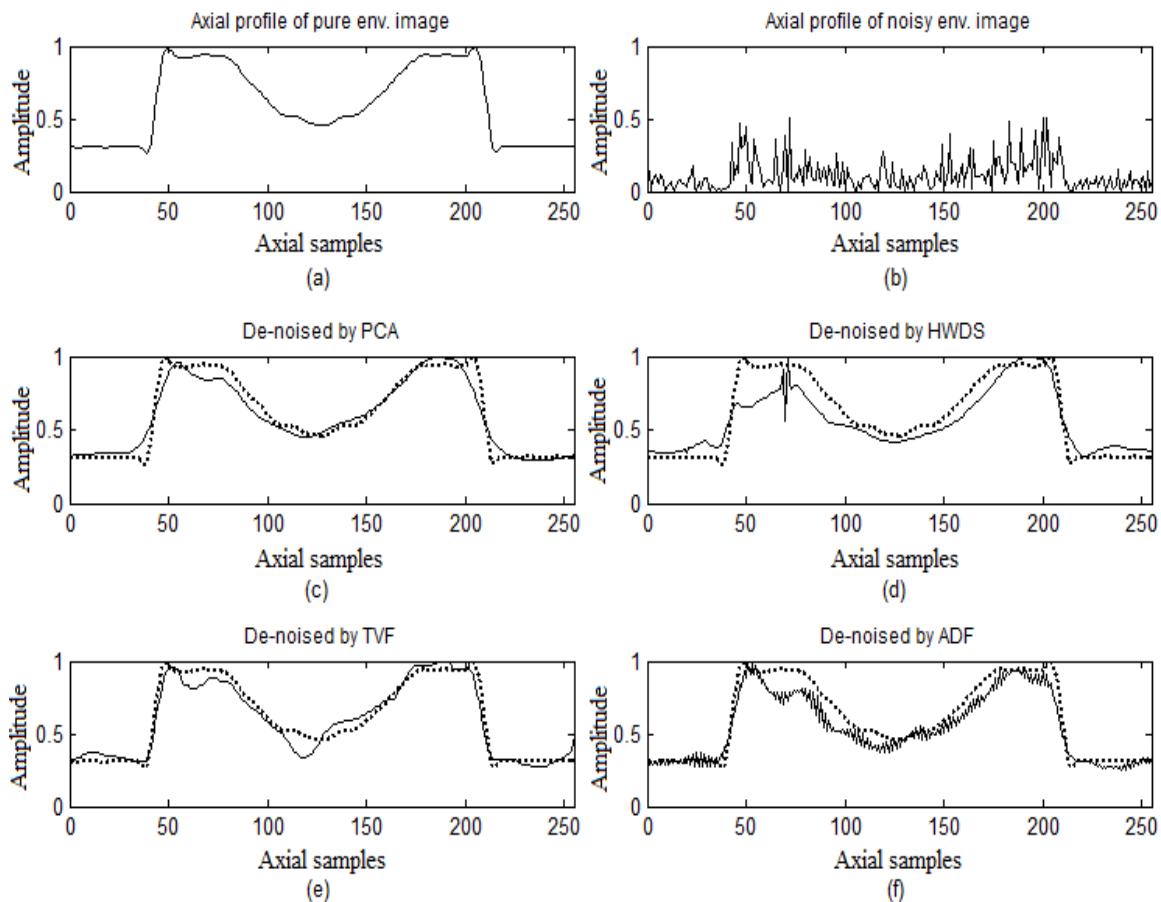
FIGURE 3: Comparison of the axial profiles of the simulated phantom images taken from the centers of the original (a) and noisy (b) images and from the centers of the despeckled images using PCA (c), HWDS (d), TVF (e), and ADF (f) methods. The dotted lines in (c) to (f) are the profile in (a).

3.2 Tissue Mimicked Image

For this simulation, the amplitude profile of the scatterers is weighted by a white Gaussian noise field in order to mimic the tissue reflectivity function of the scatterers. The difference between this simulation and the previous one is that the multiplicative noise is interred into the image to mimic the reflectivity function rather than interred to corrupt the undecimated pure 2D envelope image. In addition, a single tumor is also simulated as shown by the circular white region at the center of the image of Fig. 6. For this simulation, the Field II Program with a linear array transducer of 3.5 MHz center frequency and 100 MHz sampling frequency was used. The scatterer map consisted of 3750 scatterers per cm^2. We generate 64 scan lines with a axial resolution of 1024 samples per line and a lateral resolution of 0.312 mm. Each scan line is decimated from 1024 to 128 to yield a 128×64 image, as shown in Fig. 6. Note that the size of the image is different from that in the previous simulation. HWDS is used with 8 Daubechies vanishing moments and 8 decomposition levels. For the TVF, λ is set to 400 and the number of iterations is also set to 300. The number of iteration above 300 would blur the image. For the ADF, λ is set to the maximum of 0.25 with the number of iterations set to 50, and the conduction coefficient is set to 30. The option of favoring wide regions over small ones is chosen for the ADF. The PCA-based proposed approach is used with (16/8-1), denoting a segment size of 16×8 with one eigenvector.

The noise free phantom image before weighted by the white Gaussian noise and the speckle noisy version after weighted are shown in Fig. 6-a and b, respectively. Note that to display the image in the correct spatial aspect ratio, the images are interpolated from 128×64 to 128×256. Fig. 6 also demonstrates a visual comparison between the denoising techniques. As can be seen from Fig. 6-d, the image after despeckled using the HWDS method still contains speckle noise.

The result from the TVF method in Fig. 6-e shows that the size of the inclusion seems to be smaller than the true size, especially in the axial direction (the vertical axis). In contrast to the result from the ADF method in Fig. 6-f, the size of the inclusion seems to be larger than the true size, especially in the lateral direction (the horizontal axis). Furthermore, the background of the despeckled image from the ADF method contain high and elongated hills along the lateral direction that usually connected to the inclusion.
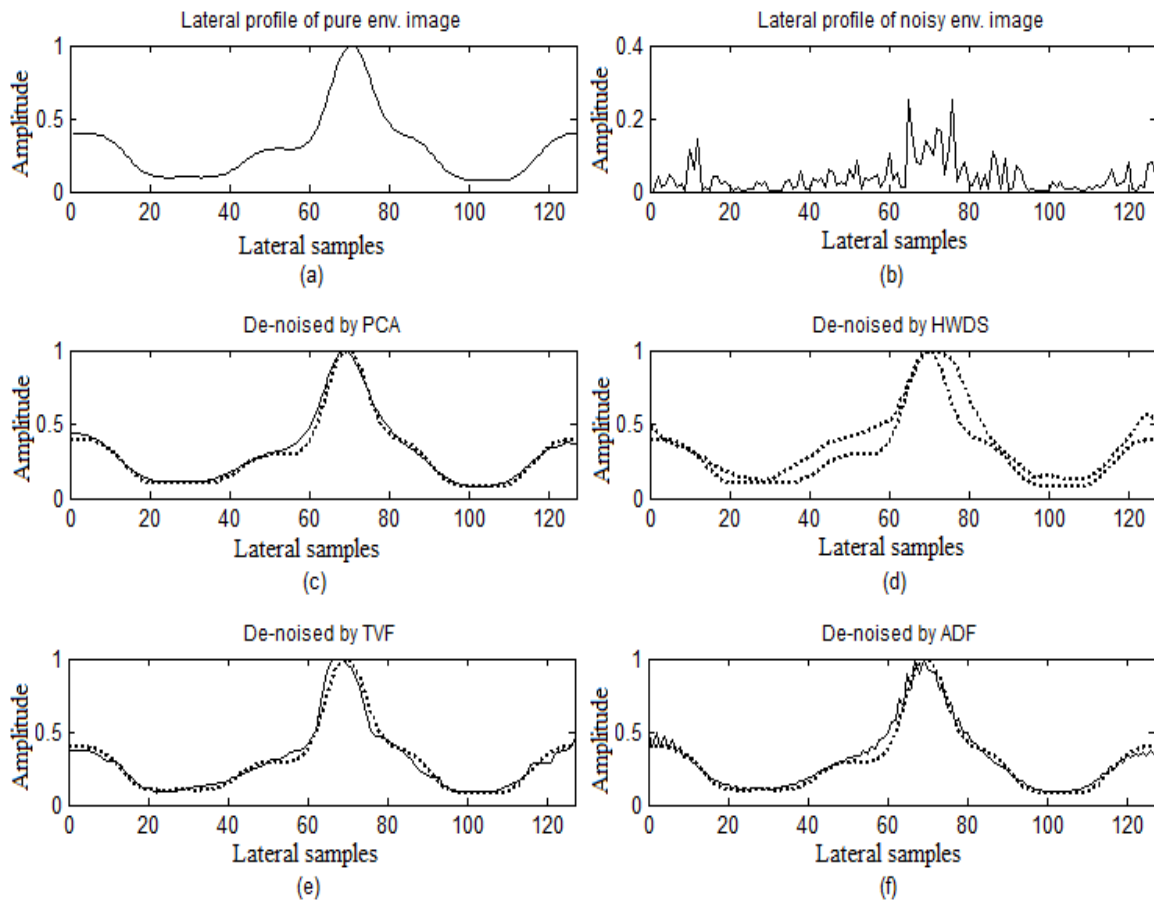

FIGURE 4: Comparison of the lateral profiles of the simulated phantom images taken from the centers of the original (a) and noisy (b) images and from the centers of the despeckled images using PCA (c), HWDS (d), TVF (e), and ADF (f) methods. The dotted lines in (c) to (f) are the profile in (a).

Fig. 7 plots a performance comparison between the denoising techniques. The proposed PCA method provides higher β, SNR, and PSNR than other methods. However, the S-SNR from the proposed approach comes in the third place after that from the TVF and the ADF methods. In agreement with the results obtained for the simulated phantom image, through the plots in Fig. 6-c and Fig. 7, the edge preservation and maximum cleaning of speckle noise obtained can be seen through the proposed PCA-based approach as compared to the other denoising schemes.

The comparisons of the axial and lateral profiles are also shown in Fig. 8 and Fig. 9, respectively. These profiles are taken from the centers of the original and noisy images in Fig. 6-a and b and

from the centers of the despeckled images using PCA, HWDS, TVF, and ADF methods in Fig. 6-c to d. The profile from the original image in (a) is also plotted as dotted lines on the same axes of the profiles from the despeckled images in (c) to (f). In general, the PCA-based approach has provided closer profiles to the original ones except for the lateral profile provided by TVF in Fig. 9-e where the lateral length of the simulated tumor is better preserved. However, in Fig. 8-c the PCA has preserved the axial length of the simulated tumor better than the TVF in Fig. 8-e. In agreement with the results provided in [8], Fig. 8-d and Fig. 9-d also show that HWDS is less efficient in removing the speckle noise. While the ADF performance looks close to the PCA performance in Fig. 8 and in Fig. 9, the calculation of the mean square error of the corresponding profiles has showed that PCA profiles are closer to the original ones than the ADF profiles.
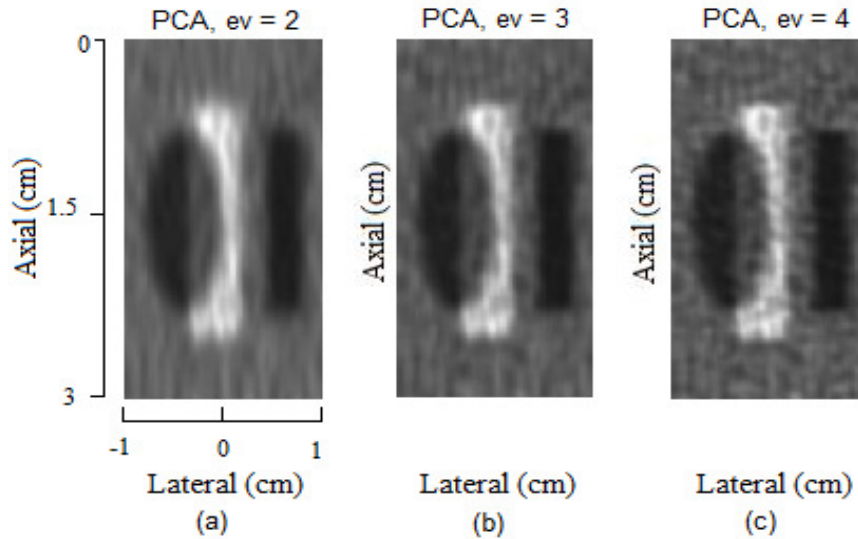
FIGURE 5: Comparison of the despeckled images using the PCA method with different numbers of principle components: ev = 2 (a), 3 (b), and 4 (c). The segment size is 16 × 8. Note that the horizontal and vertical axes represent the axial and lateral axes, respectively (the images are transposed).

The effective number of the principle components used in our PCA method is also investigated for the tissue mimicked image. The number of principle eigenvectors is changed to 2, 3, and 4 eigenvectors. The size of the segment is 16 × 8, similar to the previous experiment. The images after despeckling are shown in Fig. 10. In agreement with the results obtained for the simulated phantom image, the higher the number of eigenvectors the more dominant the speckle noise becomes. More spatial information is provided by the fewer number of eigenvectors.

To show the effect of our PCA-based approach parameters (q/p-ev) on the image quality measures (α, β, S-SNR, SNR, and PSNR), the simulated tissue mimicking image is despeckled with every possible combination of the parameters (q/p-ev), where q = {8, 16, 32}, p = {8, 16, 32}, and ev = {1, 2, 3}. The image size of 128 × 64 as used in the previous experiment is chosen.

Table I lists the PCA-based approach parameters versus the image quality measures. The ranks are also shown in the parentheses following the image quality measures. The summations of these ranks are also calculated and put in the last column with their rank in ascending order in the parentheses. Better α values (or lower number), which indicate higher resolution, seem to come from the parameters that have smaller segment sizes and more principle eigenvectors used (as shown in the second column of Table 1).

For β values, where a larger β indicates a better edge preservation of the denoising method, the segment size, both q and p parameters, seems to affect this quality measure. Larger segment sizes in the axial direction seem to provide better β. In contrast, smaller segment sizes in the

lateral direction seem to provide better β. This can be seen from the results of the parameters (32/8-1) that rank 4th in β from 27 sets of the parameters and the parameters (8/32-1) that rank 23rd. Using one principle eigenvectors seems to provide better β if the segment size is set as recommended above. This can be seen from the results of the parameters (32/8-1), (32/8-2), and (32/8-3) have rank 4th, 12th, and 9th.
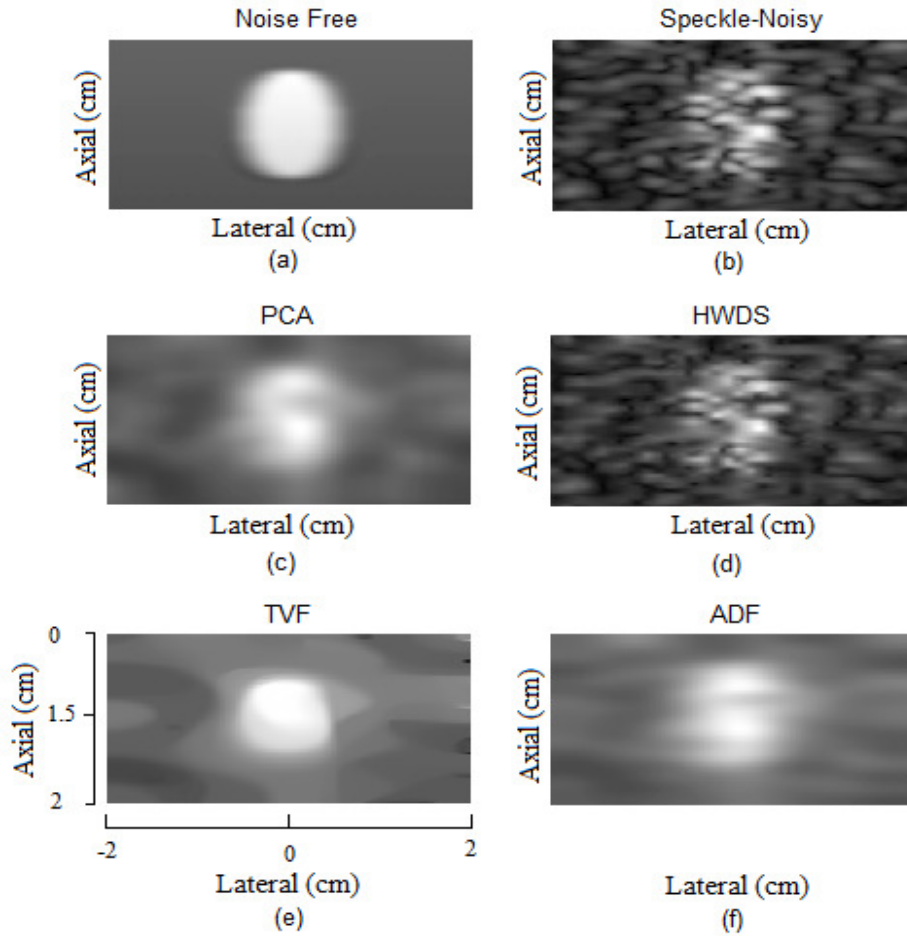
FIGURE 6: Tissue mimicking images: a noise-free envelope image (a), a speckle noisy image (b), and the images after despeckling using PCA (c), HWDS (d), TVF (e), and ADF (f) methods. Note that the horizontal and vertical axes represent the lateral and axial axes, respectively, and their representations are different from those in Fig. 1.
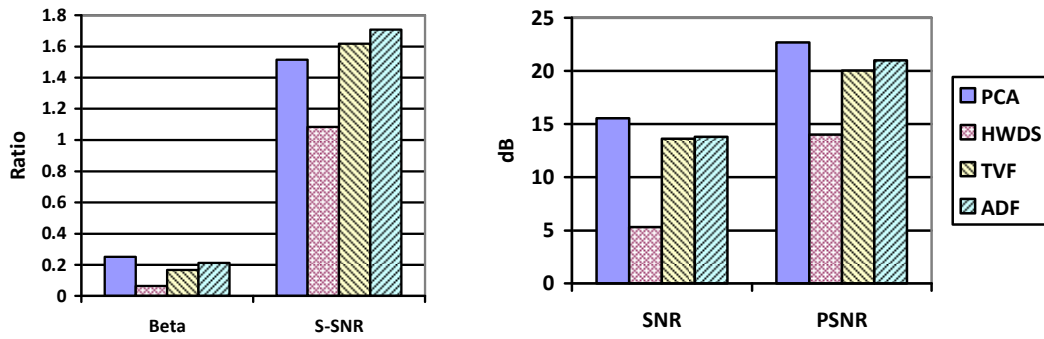
FIGURE 7: Performance comparison of denoising schemes when applied to the tissue mimicked image. Vertical axis represents the magnitude in dB for SNR and PSNR while the magnitude is of no unit for Beta and S-SNR.
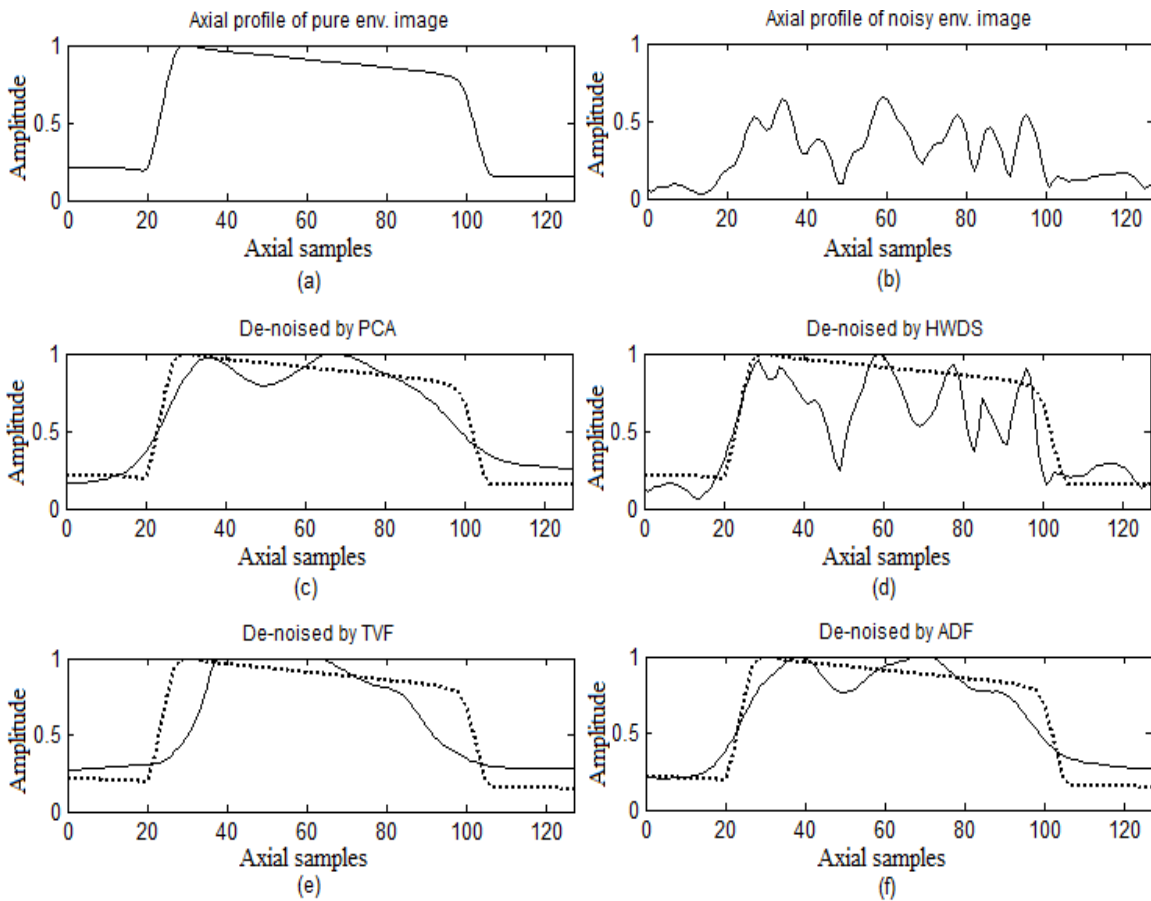
FIGURE 8: Comparison of the axial profiles of the tissue mimicking images taken from the centers of the original (a) and noisy (b) images and from the centers of the despeckled images using PCA (c), HWDS (d), TVF (e), and ADF (f) methods. The dotted lines in (c) to (f) are the profile in (a).

For S-SNR, larger segment sizes and smaller number of principle components used seem to provide better S-SNR values, as can be seen from the results of the parameters (32/32-1), (32/32-2), and (32/32-3), that rank 1st, 7th, and 11th, respectively.

For SNR and PSNR, the effects of the despeckling parameters on these image quality measures seem to be the same. The ranks 1st, 2nd, and 3rd for each measure are from the same parameters (16/32-3), (16/16-2), and (16/8-1), respectively. The large segment sizes in the lateral direction need more principle eigenvectors to obtain better SNR and PSNR. The segment size of 16 pixels in the axial direction ($q = 16$) seem to optimize these image quality measures.

The tissue mimicking images after despeckling using the proposed PCA method with some sets of parameters in Table I are shown in Fig. 11. As shown, the despeckled images from the parameter (16/32-3), (16/16-2), and (16/8-1), in the middle row of the images in Fig. 11 are the best in cleaning the speckles and also in preserving the edge of the inclusion.

3.3 Experimental Results

Real RF data is obtained for the experimental scanner RASMUS (Department of Electrical Engineering, Technical University of Denmark) -- also described in [22] -- at the time of peak systole of a carotid artery for a healthy 30 year old male. The imaging protocol used to collect the human data was approved by the Ethics committee on Biomedical Experiments for Copenhagen and the subject provided informed consent. The transducer is a B-K 8812 linear array transducer with 6.2 MHz linear array probe, 40 MHz sampling frequency and 5 MHz center frequency. The RF data are composed of 64 RF lines with 1024 samples per line. For displaying in a correct spatial aspect ratio, the image is decimated in the axial direction and is interpolated in the lateral direction to yield a 256×256 image size as shown in Fig. 12.

In order to investigate the denoising efficiency of the proposed approach, as well as to show the effect of decimation in removing parts of the noise and consequently its effect on the performance of the denoising schemes, 3 different image sizes of 512×64, 256×64, and 128×64, resulting from decimation by factors of 2, 4, and 8 in the axial directions, are despeckled using the PCA, HWDS, TVF, and ADF methods. Their parameters are shown in Table II. The visual performance of these despeckling methods is shown in Fig. 13. Note that for the displaying purpose, the image lateral dimensions are interpolated to match their axial dimensions, i.e., 512×512, 256×256, and 128×128 image sizes. The plots in Fig. 14 show the numerical performance of these despeckling methods.
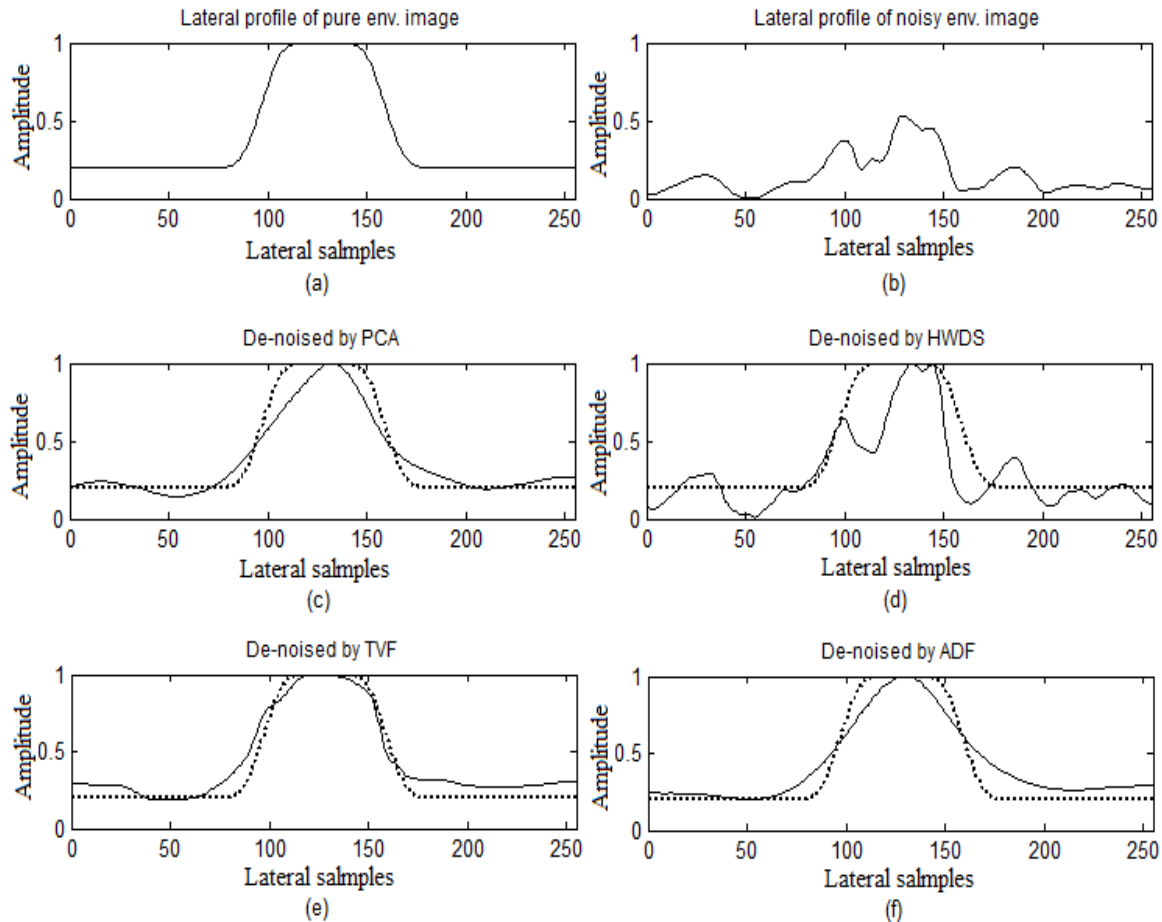
FIGURE 9: Comparison of the lateral profiles of the tissue mimicking images taken from the centers of the original (a) and noisy (b) images and from the centers of the despeckled images using PCA (c), HWDS (d), TVF (e), and ADF (f) methods. The dotted lines in (c) to (f) are the profile in (a).

Through these different decimation examples, it can be clearly observed how the decimation of the ultrasound image has a direct impact on the performance of the denoising scheme. Effect of decimation on the performance of the HWDS, TVF and ADF methods can be visually compared in Fig. 13. It can also be noticed in Fig. 14 in terms of the increasing values of α while increasing the decimation factors from 2 to 8. This implies that higher decimation factors generally reduce the despeckled image resolution. In contrast, the S-SNR values are very similar for these image sizes, except for the HWDS that the S-SNR is gradually increasing. Therefore, the decimation factor does not impact the S-SNR of the images despeckled using the PCA, TVF, and ADF method; however, higher decimation factors help the HWDS method to improve the S-SNR results.
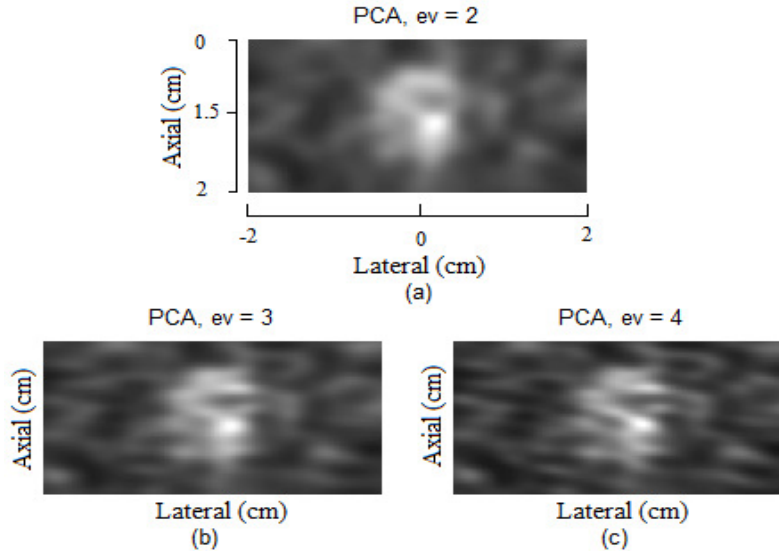
FIGURE 10: Comparison of the despeckled images using the PCA method with different numbers of principle components: *ev* = 2 (a), 3 (b), and 4 (c). The segment size is 16 × 8. Note that the horizontal and vertical axes represent the lateral and axial axes, respectively.
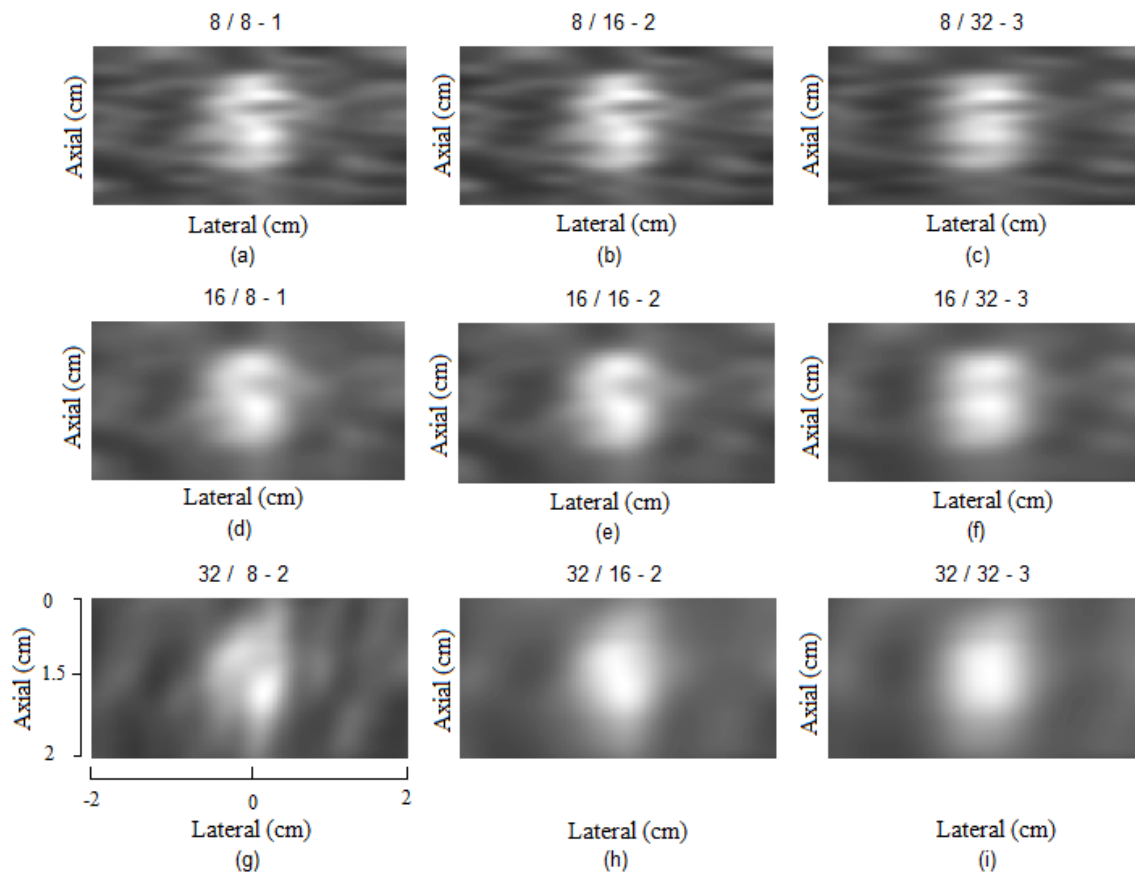

FIGURE 11: The denoising performance of the PCA-based approach for different parameters (*q/p-ev*), where *q* is the segment size in the axial direction, *p* is the segment size in the lateral direction, and *ev* is the number of the principle eigenvectors used.

| q/p-ev	α		β		S-SNR		SNR		PSNR		Sum Rank	
8/8-1	0.3400	(10)	0.1091	(19)	1.4339	(16)	13.7227	(6)	21.0744	(5)	56	(9)
8/8-2	0.0831	(2)	0.1230	(18)	1.1923	(26)	6.8194	(22)	15.4807	(22)	90	(22)
8/8-3	0.0587	(1)	0.0939	(22)	1.1385	(27)	6.0404	(24)	14.7488	(24)	98	(25)
8/16-1	0.7478	(22)	0.1055	(20)	1.9680	(6)	10.4405	(15)	18.3838	(15)	78	(17)
8/16-2	0.2902	(8)	0.1306	(16)	1.3468	(20)	13.2858	(10)	20.6813	(9)	63	(12)
8/16-3	0.1217	(4)	0.1353	(15)	1.2243	(24)	8.5016	(19)	16.8057	(19)	81	(18)
8/32-1	0.6240	(16)	0.0554	(23)	2.9884	(3)	0.5456	(27)	8.7126	(25)	94	(24)
8/32-2	0.9285	(24)	0.0970	(21)	1.6538	(10)	10.9291	(13)	18.8886	(14)	82	(19)
8/32-3	0.4368	(13)	0.1967	(7)	1.3598	(19)	12.5929	(11)	20.4564	(10)	60	(10)
16/8-1	0.5542	(15)	0.2504	(6)	1.5137	(13)	15.5510	(3)	22.6982	(3)	40	(1)
16/8-2	0.1613	(5)	0.1674	(11)	1.2872	(22)	9.1980	(17)	17.5949	(17)	72	(15)
16/8-3	0.1207	(3)	0.1245	(17)	1.2114	(25)	7.5921	(20)	16.1847	(20)	85	(20)
16/16-1	0.9581	(25)	0.3465	(2)	2.0599	(5)	8.5137	(18)	17.0704	(18)	68	(14)
16/16-2	0.5110	(14)	0.2670	(5)	1.4173	(18)	16.2386	(2)	23.0961	(2)	41	(3)
16/16-3	0.2233	(6)	0.1800	(10)	1.3099	(21)	11.0315	(12)	19.0029	(12)	61	(11)
16/32-1	0.6902	(21)	0.0000	(25)	3.1351	(2)	1.6217	(26)	7.6727	(26)	100	(26)
16/32-2	1.0000	(26)	0.0448	(24)	1.7101	(8)	9.2392	(16)	17.7663	(16)	90	(22)
16/32-3	0.6472	(18)	0.3054	(3)	1.4263	(17)	16.5988	(1)	23.3503	(1)	40	(1)
32/8-1	0.6589	(19)	0.2673	(4)	1.6698	(9)	13.4351	(9)	20.4327	(11)	52	(5)
32/8-2	0.2911	(9)	0.1569	(12)	1.4372	(15)	13.4930	(8)	20.8241	(8)	52	(5)
32/8-3	0.2272	(7)	0.1879	(9)	1.2816	(23)	10.7855	(14)	18.8960	(13)	66	(13)
32/16-1	0.9260	(23)	0.6001	(1)	2.2816	(4)	6.7772	(23)	15.1996	(23)	74	(16)
32/16-2	0.6294	(17)	0.1419	(14)	1.5588	(12)	13.8496	(5)	21.1800	(4)	52	(5)
32/16-3	0.3795	(12)	0.1507	(13)	1.4617	(14)	13.6787	(7)	21.0017	(7)	53	(8)
32/32-1	0.3737	(11)	0.0000	(25)	3.8110	(1)	1.8763	(25)	7.3329	(27)	89	(21)
32/32-2	1.0000	(26)	0.0000	(25)	1.8563	(7)	7.5074	(21)	15.8430	(21)	100	(26)
32/32-3	0.6812	(20)	0.1948	(8)	1.5710	(11)	14.0827	(4)	21.0244	(6)	49	(4)

TABLE 1: Performance of PCA-based approach when applied to the simulated tissue mimicked image. Note: The numbers in the parentheses are the rank in the descending order, except for the first and the last column in the ascending order.

The increasing value of α can also imply less speckle noise remained after despeckling. This is clearly seen by comparing the despeckled images using the HWDS method in the 2nd column of Fig. 13 and their α values on the bar graphs in Fig. 14. As can be seen in the 2nd column of Fig. 13, the speckle noise is diminishing from the images while the α values are increasing. Therefore, higher α values could imply lower image resolution and less speckle noise remaining after despeckling.

From Fig. 13 and Fig. 14, the results from the PCA method can be compared to those from other methods in terms of image visual quality, α values, and S-SNR values. For the image visual quality, the results from the PCA method are comparable to those from the TVF and ADF methods. The TVF method seems to provide better edges of the carotid artery for the images of 512×64 and 256×64 image sizes. However, some speckle artifacts are left on the top border of the artery on the image of 128×64 image size (as shown in the 3rd row and the 3rd column of Fig. 13).
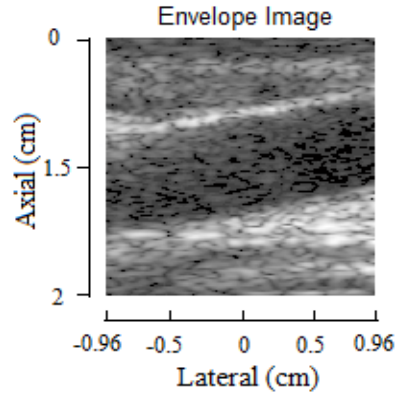
FIGURE 12: A carotid artery image before despeckling. Note that the horizontal and vertical axes are the lateral and axial directions, respectively.
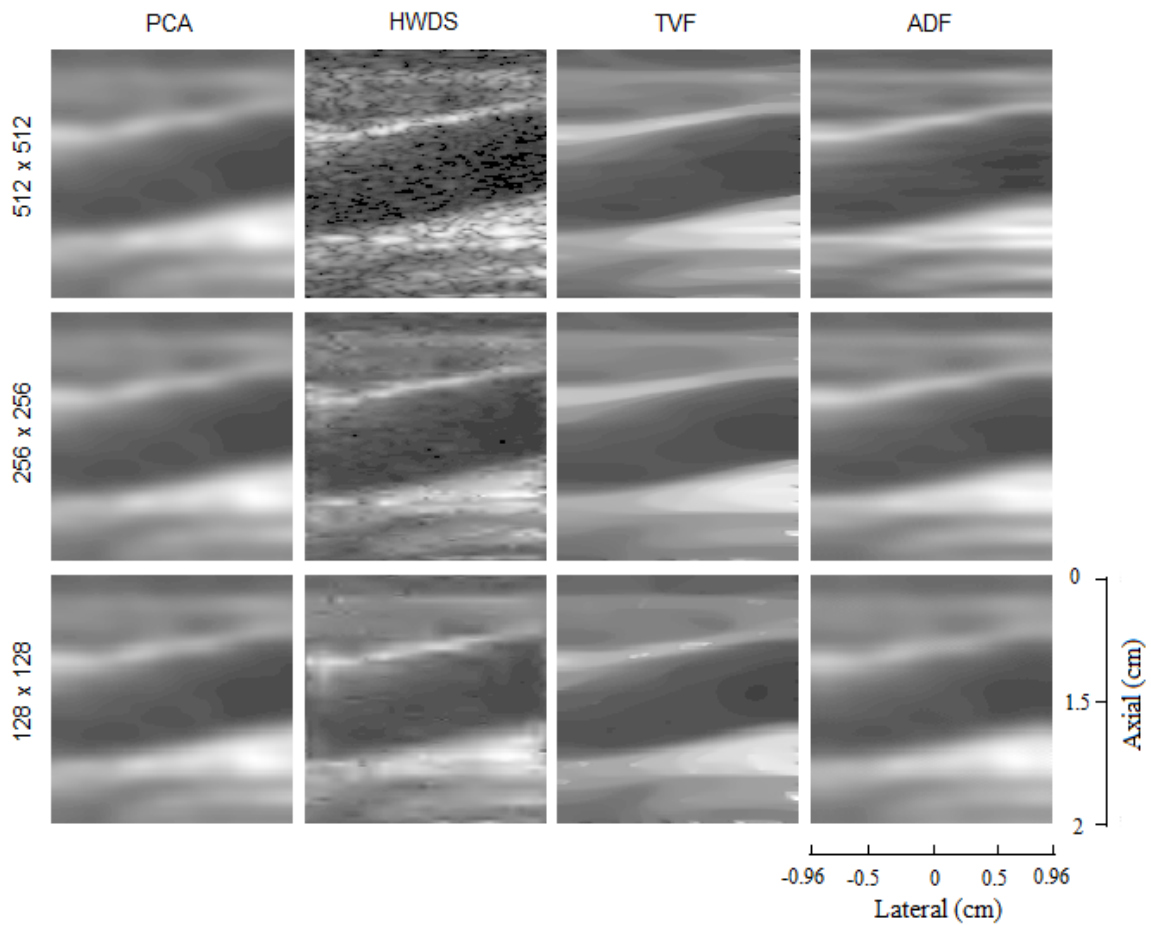
FIGURE 13: Comparison of despeckled carotid artery images using the PCA, HWDS, TVF, and ADF methods (respectively shown in 1st to 4th columns) applied on the images after decimation in the axial dimension to the sizes of 512×64, 256×64 and 128×64 (respectively shown in the 1st to 3rd rows). Note that for displaying purpose the images are interpolated in the lateral dimensions to match their axial dimensions. The horizontal and vertical axes are the lateral and axial directions, respectively.

Method	Parameters	Image size 512 × 64	Image size 256 × 64	Image size 128 × 64
PCA	Segment size	32 × 8	16 × 8	8 × 8
	Eigenvector used	1	1	1
HWDS	Wavelet function	Daubechies	Daubechies	Daubechies
	Vanishing moment	8	8	4
	Decomposition level	8	8	4
TVF	λ	500	500	400
	Iteration number	300	300	150
ADF	λ	0.25	0.25	0.25
	Iteration number	60	50	30
	Conduction Coefficient	30	25	25
	Favoring region	Wide	Wide	Wide

TABLE 2: Despeckling parameters used in the carotid artery images with different image sizes.
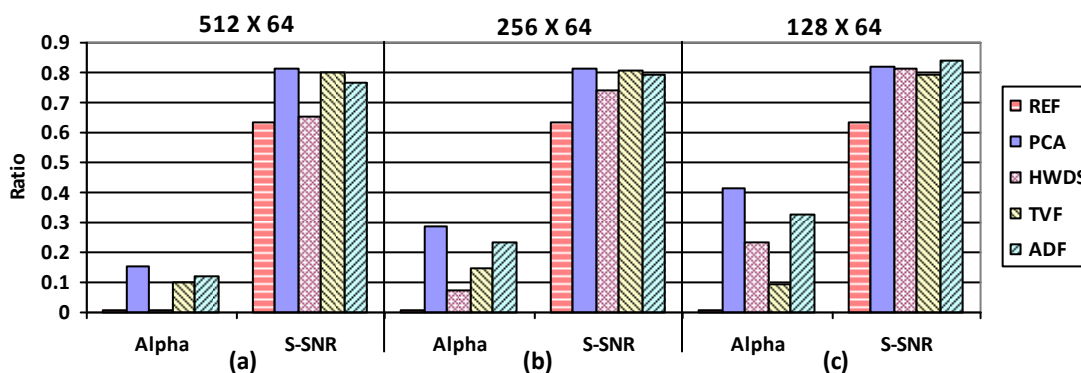

FIGURE 14: The bar graphs of the alpha and S-SNR values measured on carotid artery images of 512 × 64, 256 × 64, and 128 × 64 image sizes (respectively from a to c) before despeckling (REF) and after despeckling using the PCA, HWDS, TVF, and ADF methods. Vertical axis represents the magnitude.

The image visual quality of the results from the PCA, TVF, and ADF methods is far better than that from the HWDS method. For the S-SNR values, the despeckled images from the PCA method have better S-SNR values than most of those from the other methods, except for the S-SNR value from the ADF method applied on the image of 128 × 64 image size is better than those from the PCA method. For the α values, the despeckled images from the PCA method have higher α values than the other methods. The α parameter can be improved (lower α) by using more than one principle component per block but that will be on the account of the S-SNR. However, unlike the other denoising methods in this paper which provide better resolution accompanying reduction in the despeckling efficiency when they are applied to larger image sizes, the proposed PCA method improves the resolution while maintaining the superiority of speckle removal. Improving α while maintaining high S-SNR is observed for the PCA when moving from small to larger image sizes; from c to a in Fig. 14, or more clearly by comparing the despeckling performance of the methods for the 256 × 64 image size with the 512 × 64 image size. In general, the PCA method is a powerful speckle removing scheme regardless of the decimation factor or image size. Once the proper denoising block size is selected, the PCA-based approach provides high quality denoising results.

To further investigate the effective number of the principle components used in the PCA method on real ultrasound data, the carotid artery image of 256×64 image size is despeckled using the segment size of 16×8 and 2, 3, and 4 principle components, i.e., the parameters of (16/8-2), (16/8-3), and (16/8-4). The despeckled images are shown in Fig. 15. As expected, the higher number of principle components used, the more speckle noise becoming dominant. These results are in accordance with the simulation results previously shown.

The choice for the $q \times p$ denoising block size in this paper is based by default on the image size itself and the size of the speckle noise clusters. It follows $M \cdot \lfloor \sqrt{n} \rfloor_8 \times \lfloor \sqrt{m} \rfloor_8$ rule, where M is equal to 1 for small noise clusters and equal to 2 for large noise clusters; $\lfloor \sqrt{\cdot} \rfloor_8$ means the square root value is floored to the nearest multiple of eight; and n and m are the number of pixels in the axial and lateral dimensions of the image. For example, for the simulated phantom image of 256×128 image size in Fig. 1-b showing small noise clusters, therefore, the denoising block size is set to 16×8 ($M = 1$). For the simulated tissue mimicking image in Fig. 6-b after decimating its size to 128×64, the image shows large noise clusters; therefore, the block size is set to 16×8 ($M = 2$). For the carotid artery image in Fig. 12 after decimating its size to 128×64, the image shows small noise clusters; therefore, the block size is set to 8×8 ($M = 1$).

The complexity of these despeckling methods can be compared as follows. For the PCA method, there are three main stages. The first stage is to find N covariance matrices of vectors of $q.p$ length, where N is the number of image pixels and $q \times p$ is the segment size. Finding a covariance matrix of a vector requires the complexity of L^2, where L is the length of the vector. The complexity of the first stage is Nq^2p^2. From the rule to select the block size described above, $q^2p^2 \approx nm = N$. Therefore the complexity of the first stage is N^2. The second stage is to find the maximum eigenvector of the averaged covariance matrix. This requires the use of an eigen decomposition procedure and a sorting procedure. The eigen decomposition procedure is dominant and its complexity is M^3, where M is the number of elements in the matrix [25]. Therefore, the complexity of the second stage is $(q^2p^2)^3 \approx N^3$. Finally, the third stage is to projecting or filtering N vectors of $q.p$ length by a projection matrix of q^2p^2 size. This third stage requires a complexity of $NNq.p \approx N^{5/2}$. From these complexity approximations showing that the second stage is dominant, the complexity of the PCA method is N^3 and it is depending on the eigen decomposition procedure.

The complexity of the HWDS, TVF, and ADF methods can be approximated as follows. HWDS, wavelet decomposition and reconstruction require a complexity of $N \log N$ [26]. The TVF and ADF require a complexity of N for each iteration [27]. Note that the number of iteration is small compared to N. To enhance the performance of HWDS, TVF, and ADF there are two main preprocessing stages [6], which are point spread function estimation and outlier shrinkage stage. Point spread function estimation requires a complexity of $N \log N$ [28], while the outlier shrinkage stage requires a complexity of N. Note that the median filter size used in the outlier shrinkage is small compared to N. Therefore, the complexity of these despeckling methods including preprocessing is $N \log N$, which is lower than N^3 of the PCA method. However, the complexity of the PCA method could be reduced if we despeckled the image in the axial and lateral directions separately. Since the length of the vector for the covariance calculation is reduced to q or p for each direction. Therefore, the complexity could be reduced to $N^{3/2}$ and it is because of the domination of the eigen decomposition procedure. Nevertheless, this number is still larger than $N \log N$.
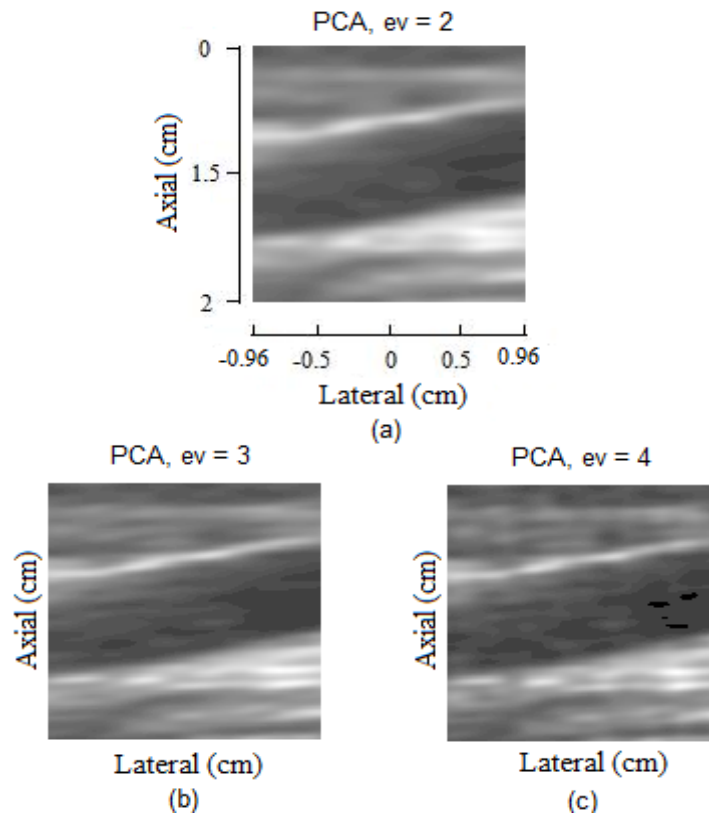
FIGURE 15: Comparison of the despeckled images using the PCA method with different numbers of principle components: ev = 2 (a), 3 (b), and 4 (c). The image size before despeckling is 256 × 64 and the segment size is 16 × 8. Note that the horizontal and vertical axes are the lateral and axial directions, respectively.

4. CONCLUSIONS

A PCA-based approach to filter out multiplicative noise from ultrasound images has been presented in this paper. It segments the envelope image into small overlapping blocks, finds a subspace representation of these blocks via principle component analysis, projects them back to the subspace, and averages the projections. The size of the block is dependent on the original size of the image and the size of the noise cluster found in the image. The proposed PCA-based approach outperforms many existing denoising approaches such as the homomorphic wavelet despeckling [4], the total variation filtering [10], and the anisotropic diffusion filtering [9] in both simulation and real ultrasound data. In terms of image resolution (α) the PCA-based approach lags the other denoising schemes. However, the S-SNR from PCA is the best for higher resolution (less decimated) images. It has been verified that, per segment size, very few principle components (in most cases the first or the first and the second principle components) are needed to represent the true signal. The proposed method depends solely on the size of the image and the number of the principle components used, while many parameters need to be adjusted for the other methods in order to obtain acceptable denoising results. Moreover, no preprocessing is needed for the proposed method, while the other methods need many preprocessing stages, such as decorrelating the speckle noise samples and then removing the outliers from the log transformed speckle noise [6]. It has been shown that the prior decimation factors performed on the noisy images have no effect on the despeckling quality of the results. In contrast to the homomorphic wavelet despeckling needs high decimation factors to improve the results. However, our approach needs to be optimized to improve the computational time and reduce the complexity of the algorithm.

5. FUTURE RESEARCH DIRECTIONS

Optical Coherence Tomography (OCT) is similar to the principle of ultrasound in the sense that OCT images are formed from the envelope of the measured interference signal. It has been shown that computation of the absolute magnitude of the signal for measurement of the envelope is a nonlinear process that destroys phase information. Processing the partially coherent OCT signals in the complex domain has provided the opportunity to correct phase aberrations responsible for speckle noise in OCT images. One of the future research directions for developing additional models for ultrasound image despeckling is to investigate the phase and spectra of the received ultrasound echo signals that are usually ignored when the magnitudes of the complex signals are being solely considered.

6. ACKNOWLEDGMENT

7. REFERENCES

[1]   X. Zong, A. F. Laine, and E. A. Geiser, "Speckle reduction and contrast enhancement of echocardiograms via multiscale nonlinear processing.," IEEE Trans. Med. Imaging, vol. 17, no. 4, pp. 532–40, Aug. 1998.

[2]   A. Achim, A. Bezerianos, and P. Tsakalides, "Novel Bayesian multiscale method for speckle removal in medical ultrasound images.," IEEE Trans. Med. Imaging, vol. 20, no. 8, pp. 772–83, Aug. 2001.

[3]   L. Gagnon, A. Jouan, R. De, L. M. Canada, and A. Royalmount, "Speckle Filtering of SAR Images - A Comparative Study Between Complex-Wavelet-Based and Standard Filters," 1997.

[4]   S. Gupta, R. C. Chauhan, and S. C. Saxena, "Homomorphic wavelet thresholding technique for denoising medical ultrasound images.," J. Med. Eng. Technol., vol. 29, no. 5, pp. 208–14.

[5]   T. Loupas, W. N. McDicken, and P. L. Allan, "An adaptive weighted median filter for speckle suppression in medical ultrasonic images," IEEE Trans. Circuits Syst., vol. 36, no. 1, pp. 129–135, Jan. 1989.

[6]   O. V. Michailovich and A. Tannenbaum, "Despeckling of medical ultrasound images," IEEE Trans. Ultrason. Ferroelectr. Freq. Control, vol. 53, no. 1, pp. 64–78, Jan. 2006.

[7]   R. K. Mukkavilli, J. S. Sahambi, and P. K. Bora, "Modified homomorphic wavelet based despeckling of medical ultrasound images," in 2008 Canadian Conference on Electrical and Computer Engineering, 2008, pp. 000887–000890.

[8]   E. Nadernejad, "Despeckle Filtering in Medical Ultrasound Imaging," Contemp. Eng. Sci., vol. 2, no. 1, pp. 17–36, 2009.

[9]   P. Perona and J. Malik, "Scale-space and edge detection using anisotropic diffusion," IEEE Trans. Pattern Anal. Mach. Intell., vol. 12, no. 7, pp. 629–639, Jul. 1990.

[10] L. I. Rudin, S. Osher, and E. Fatemi, "Nonlinear total variation based noise removal algorithms," Phys. D Nonlinear Phenom., vol. 60, no. 1–4, pp. 259–268, Nov. 1992.

[11] Y. Wang, X. Fu, L. Chen, S. Ding, and J. Tian, "DTCWT based medical ultrasound images despeckling using LS parameter optimization," 2013 IEEE Int. Conf. Image Process., pp. 805–809, Sep. 2013.

[12] M.-S. Lee, C.-L. Yen, and S.-K. Ueng, "Speckle reduction with edges preservation for ultrasound images: using function spaces approach," IET Image Process., vol. 6, no. 7, p. 813, 2012.

[13] Y. Yu and S. T. Acton, "Speckle reducing anisotropic diffusion.," IEEE Trans. Image Process., vol. 11, no. 11, pp. 1260–70, Jan. 2002.

[14] G. M. Henebry, "Advantages of principal components analysis for land cover segmentation from SAR image series," in Third ERS Symposium on Space at the service of our Environment, 1997, pp. 14–21 .

[15] J.-S. Lee and K. Hoppel, "Principal components transformation of multifrequency polarimetric SAR imagery," IEEE Trans. Geosci. Remote Sens., vol. 30, no. 4, pp. 686–696, Jul. 1992.

[16] J. Shlens, A Tutorial on Principal Component Analysis. 2009.

[17] J. F. Al-Asad, A. Moghadamjoo, and L. Ying, "Ultrasound image de-noising through Karhunen-Loeve (K-L) transformwith overlapping segments," in 2009 IEEE International Symposium on Biomedical Imaging: From Nano to Macro, 2009, pp. 318–321.

[18] J. A.K, Fundamental of Digital Image Processing. NJ: Prentice-Hall, 1989, pp. 267–330.

[19] X. Hao, S. Gao, and X. Gao, "A novel multiscale nonlinear thresholding method for ultrasonic speckle suppressing.," IEEE Trans. Med. Imaging, vol. 18, no. 9, pp. 787–94, Sep. 1999.

[20] J. A. Jensen, D.- Lyngby, P. Medical, B. Engineering, and I. Technology, "Paper presented at the 10th Nordic-Baltic Conference on Biomedical Imaging : Field : A Program for Simulating Ultrasound Systems Field : A Program for Simulating Ultrasound Systems," vol. 34, pp. 351–353, 1996.

[21] J. A. Jensen and N. B. Svendsen, "Calculation of pressure fields from arbitrarily shaped, apodized, and excited ultrasound transducers.," IEEE Trans. Ultrason. Ferroelectr. Freq. Control, vol. 39, no. 2, pp. 262–7, Jan. 1992.

[22] J. A. Jensen, O. Holm, L. J. Jerisen, H. Bendsen, S. I. Nikolov, B. G. Tomov, P. Munk, M. Hansen, K. Salomonsen, J. Hansen, K. Gormsen, H. M. Pedersen, and K. L. Gammelmark, "Ultrasound research scanner for real-time synthetic aperture data acquisition," IEEE Trans. Ultrason. Ferroelectr. Freq. Control, vol. 52, no. 5, pp. 881–891, May 2005.

[23] G. Georgiou and F. S. Cohen, "Statistical characterization of diffuse scattering in ultrasound images.," IEEE Trans. Ultrason. Ferroelectr. Freq. Control, vol. 45, no. 1, pp. 57–64, Jan. 1998.

[24] D. L. Donoho, "De-noising by soft-thresholding," IEEE Trans. Inf. Theory, vol. 41, no. 3, pp. 613–627, May 1995.

[25] D. Tufts and C. Melissinos, "Simple, effective computation of principal eigenvectors and their eigenvalues and application to high-resolution estimation of frequencies," IEEE Trans. Acoust., vol. 34, no. 5, pp. 1046–1053, Oct. 1986.

[26] Y. Yue, M. M. Croitoru, A. Bidani, J. B. Zwischenberger, and J. W. Clark, "Nonlinear multiscale wavelet diffusion for speckle suppression and edge enhancement in ultrasound images.," IEEE Trans. Med. Imaging, vol. 25, no. 3, pp. 297–311, Mar. 2006.

[27] T. Brox and D. Cremers, "Iterated Nonlocal Means for Texture Restoration," no. May, pp. 13–24, 2007.

Jawad F. Al-Asad, Ali M. Reza & Udomchai Techavipoo

[28] O. Michailovich and A. Tannenbaum, "Blind Deconvolution of Medical Ultrasound Images: A Parametric Inverse Filtering Approach," IEEE Trans. Image Process., vol. 16, no. 12, pp. 3005–3019, Dec. 2007.